

SENet: Visual Detection of Online Social Engineering Attack Campaigns

Irfan Ozen*, Karthika Subramani†, Phani Vadrevu‡ and Roberto Perdisci*†

*University of Georgia

†Georgia Institute of Technology

‡Louisiana State University

Abstract—Social engineering (SE) aims at deceiving users into performing actions that may compromise their security and privacy. These threats exploit weaknesses in humans’ decision-making processes by using tactics such as pretext, baiting, impersonation, etc. On the web, SE attacks include attack classes such as scareware, tech support scams, survey scams, sweepstakes, etc., which can result in sensitive data leaks, malware infections, and monetary loss. For instance, US consumers lose billions of dollars annually due to various SE attacks. Unfortunately, generic social engineering attacks remain understudied, compared to other important threats, such as software vulnerabilities and exploitation, network intrusions, malicious software, and phishing. The few existing technical studies that focus on social engineering are limited in scope and mostly focus on measurements rather than developing a generic defense.

To fill this gap, we present *SEShield*, a framework for in-browser detection of social engineering attacks. *SEShield* consists of three main components: (i) a custom security crawler, called *SECrawler*, that is dedicated to scouting the web to collect examples of in-the-wild SE attacks; (ii) *SENet*, a deep learning-based image classifier trained on data collected by *SECrawler* that aims to detect the often glaring visual traits of SE attack pages; and (iii) *SEGuard*, a proof-of-concept extension that embeds *SENet* into the web browser and enables real-time SE attack detection. We perform an extensive evaluation of our system and show that *SENet* is able to detect new instances of SE attacks with a detection rate of up to 99.6% at 1% false positive, thus providing an effective first defense against SE attacks on the web.

1. Introduction

Social engineering (SE) encompasses a broad spectrum of attacks aimed at deceiving users into performing actions that may have important negative consequences for the security and privacy of the users themselves or their organizations [1]. These threats exploit weaknesses in humans’ decision-making processes by using tactics such as pretext, baiting, impersonation, etc. [2]. On the web, SE attacks include attack classes such as scareware [3], tech support scams [4], survey scams [5], sweepstakes [6], etc., which can result in sensitive data leaks, malware infections, and

monetary loss. For instance, US consumers lose billions of dollars annually due to various SE attacks [7].

Unfortunately, social engineering attacks remain understudied, compared to other important threats, such as software vulnerabilities and exploitation, network intrusions, malicious software, and botnets. While phishing attacks, which can be thought of as a specific subclass of SE attacks, have received significant attention [8], to the best of our knowledge no comprehensive defense framework against generic SE attacks has been proposed or evaluated.

Previous studies on SE attacks are either limited to discovering and measuring SE attack campaigns [9], [10] or to studying specific subclasses of SE attacks [4], [3], [5], [11]. Furthermore, existing practical defenses against malicious web pages mostly rely on reactive approaches that do not focus on the fundamental traits of SE attacks and tend to lag behind new threats, thus leaving many users exposed to the latest attack iterations. For instance, URL blocklist services (e.g., Google Safe Browsing [12]) focus on *where* malicious content is hosted, rather than detecting and blocking the malicious content itself. Therefore, attackers evade blocking by simply relocating their attacks to a different hosting location [9].

A recent work by Yang et al. [13] has started to address the problem of detecting and blocking web-based SE attacks by proposing an in-browser defense system named TRIDENT. However, TRIDENT narrowly focuses on detecting JavaScript code served by low-reputation ad networks that often use SE techniques, such as transparent overlays, to hijack users’ clicks and redirect them to a potentially malicious page. TRIDENT is able to detect SE webpages only indirectly, because low-tier ad network code often (but not always [9]) redirects to SE attacks. Therefore, there is a need for more generic solutions that are able to directly detect generic web-based SE attacks, even when they are not linked specifically to ad network code.

Problem Definition and Motivation: In this paper, we aim to build an in-browser defense against generic web-based Social Engineering (SE) attacks, such as *fake software downloads*, *online sweepstakes*, *fake antiviruses*, *tech support scams* (TSS), *notification permission stealing*, etc.

Although phishing may be considered as a subcategory of SE attacks, we regard phishing websites as out of scope for this work, due to their different characteristics, compared

to generic SE attacks. Specifically, the reasons for focusing on SE attacks other than phishing are as follows:

1) *SE attacks differ from phishing*: Phishing attacks typically attempt to (i) mimic a specific benign target website (e.g., an online banking site, ecommerce site, etc.) and (ii) directly ask users to submit personal information, such as login credentials, credit card or social security numbers, etc, as part of the attack. On the other hand SE attacks do not need to mimic a specific website (though in some cases they may abuse a popular brand/logo) and do not need to directly ask users to submit personal information (though they may further lead to information stealing). For instance, fake software download attacks trick the user into downloading malicious software, TSS attacks convince the user to call a fake support phone number, notification stealing attacks trick users into granting notification permission to potentially malicious websites, etc. The examples of real-world screenshots shown in Table 1 demonstrate the typical visual differences between SE and phishing attacks pages. Notice that most SE attacks do not include any input boxes, and that in many cases no specific brand or company logo is abused, whereas these properties are required in typical phishing pages.

2) *Defenses against SE attacks are critically understudied*: While there exists an extensive body of work that studies how to detect phishing web pages [8], including using visual classification [14], [15], [16], generic SE attacks remain understudied. Few previous works have addressed the problem of defending against web-based SE attacks, with a limited focus on collecting/measuring SE campaigns [9], [10] or on detecting ad network code that often leads to SE attack pages [13].

Differences Compared to Previous Work: Visual approaches that have been proposed to detect Phishing web pages [14], [15], [16] are specific to Phishing attack characteristics, which are typically not in common with generic SE attacks. For instance, VisualPhishNet [14] leverages the similarity between Phishing attack pages and a well-defined list of target benign websites (e.g., banking websites, social media sites, etc.). Phishpedia [15] focuses on detecting the misuse of a target set of logos, whereas PhishIntention [16] aims to detect the joint appearance of abused logos and credential stealing forms. However, in the case of most SE attacks there are no specific target benign pages that are mimicked, credential stealing forms are typically not present, and while logos are sometimes abused they are often significantly different than benign logos or are completely absent from many SE attack campaigns.

Unlike previous work, we aim to build a SE attack detection framework that allows us to (i) discover and collect examples of generic SE attacks served by different SE campaigns, (ii) train a deep learning-based system to visually detect future variants of SE attacks from observed campaigns, and (iii) deploy the SE attack detection model into the browser to enable real-time detection of new SE attack instances (see Figure 1). Additionally, an important objective of our work is to build a *practical* solution that could be deployed into web browsers running on a variety of

devices, including laptop and desktop computers and mobile devices.

To this end, we focus on detecting web-based SE attacks using a deep learning-based computer vision approach, which is motivated by the following main observations:

- SE attacks aim to trick users by presenting them with misleading content, and thus tend to have a *significant visual component* that must be present for such attacks to succeed.
- Large-scale SE attacks are often organized into *attack campaigns*, whereby attacks belonging to the same campaign share a common theme and thus carry similar content and visual traits.
- Recent advancements in deep learning have drastically improved the accuracy of image classification tasks, with popular deep learning frameworks now also available for languages such as JavaScript, making it feasible to build complex in-browser AI systems.

Contributions: Motivated by the observations outlined above, in this paper we make the following main contributions:

– We propose *SEShield*, a framework to enable the detection of generic web-based SE attacks. *SEShield* consists of three components: (i) a system for discovering and collecting examples of SE attack campaigns, named *SECrawler*, (ii) a deep-learning based visual classifier called *SENet*, and (iii) a browser extension named *SEGuard* that classifies web pages in real time and alerts the user when an SE attack is detected. Among these three components, most of our research efforts and contributions are dedicated to designing, implementing and evaluating the *SENet* classifier. At the same time, we also build a prototype of *SECrawler* and *SEGuard* to enable the collection of SE attacks needed to train *SENet* and to demonstrate the viability of the *SEShield* defense framework.

– We implement *SECrawler* by extending previous work [9] to discover and collect fresh examples of SE attack campaigns. We then label the collected data by employing three different human labelers and using a systematic labeling strategy to obtain high-quality ground truth, which we use to train and evaluate the *SENet* classifier. Our dataset consists of 7,484 labeled SE attack pages (captured using 30 different emulated devices and screen sizes) that belong to 74 different SE attack campaigns. We will release our dataset to the research community to enable further research in this area.

– We design *SENet* as a visual detection model that enables the classification of images of arbitrary sizes, and develop a new distributed training approach to be able to train our model with limited GPU resources. *SENet* can be deployed in the browser and is able to visually detect SE attack webpages independently of the size of the screen (or browser window) where the page is rendered.

– We conduct an extensive evaluation of *SENet* to demonstrate its ability to detect new instances of SE attacks linked to campaigns observed by *SECrawler*. We show that

TABLE 1: Examples showing the different visual characteristics of Phishing vs. generic SE attack pages.

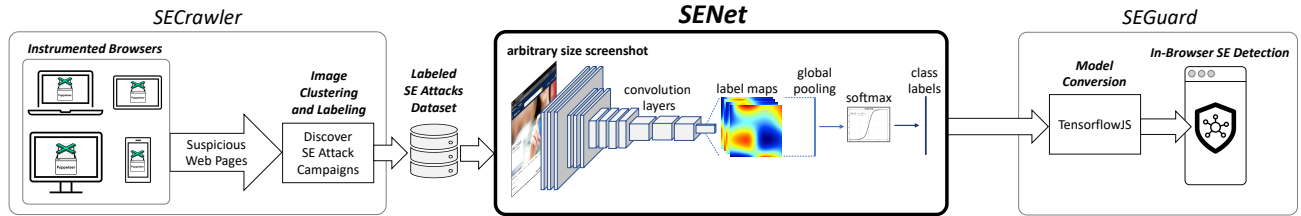
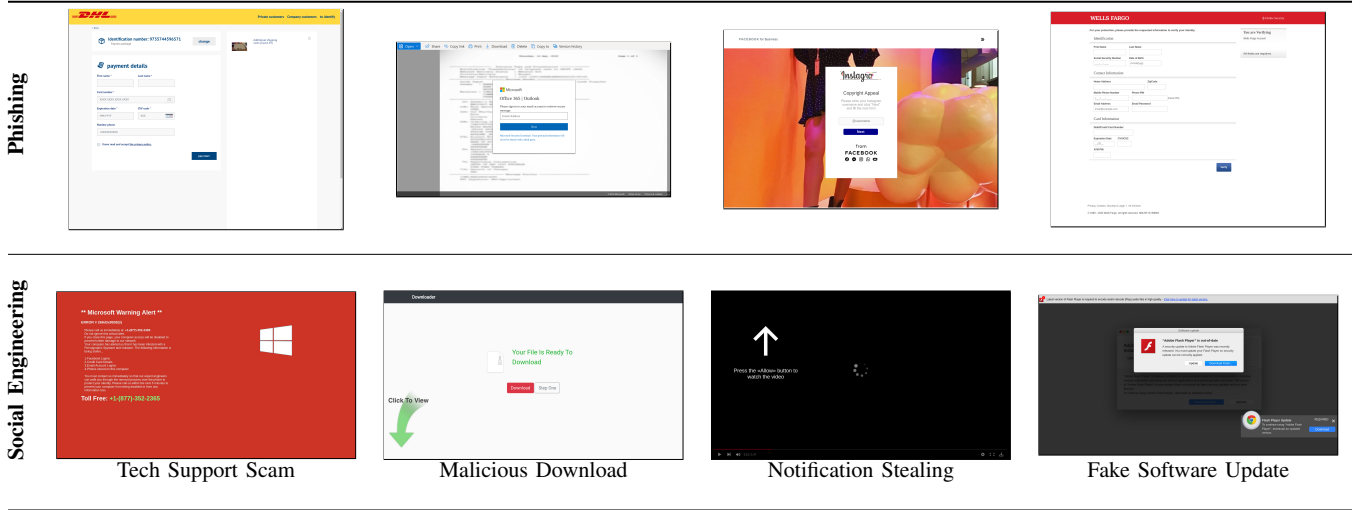


Figure 1: *SEShield* framework overview. *SENet* represents the primary contribution and main research focus of this paper. *SECrawler* and *SEGward* are implemented as early prototypes that we use for training data collection and to demonstrate the viability of *SENet* and of the entire *SEShield* defense framework to enable a practical in-browser defense against SE attacks.

SENet can accurately detect new SE attack instances with up to 99.6% recall at 1% false positive rate, that it is able to generalize to input images (i.e., webpage screenshots) related to previously unseen screen sizes, and that it is also able to generalize to detecting a number of never-before-seen SE campaigns.

– We implement a prototype of *SEGward* as a browser extension using TensorFlowJS [17] to demonstrate the utility of the entire *SEShield* framework as a practical defense against SE attack webpages. We plan to release all components of our *SEShield* framework as open-source software.

2. Framework Overview

In this section, we present an overview of our SE defense framework, named *SEShield*, which aims to offer a practical defense against generic web-based SE attacks. Figure 1 shows the three components that make up our framework: *SECrawler*, *SENet*, and *SEGward* (we introduce each component in more detail below). In this paper, we focus most of our research efforts on *SENet*, and build an early prototype of *SECrawler* and *SEGward* to enable the collection of SE attack examples and to demonstrate

the viability of *SENet* and of the entire *SEShield* defense framework.

As mentioned in Section 1, we focus on detecting SE attacks beyond phishing, such as *fake software downloads*, *scareware*, *sweepstakes*, *tech support scams*, etc. To detect SE attacks, we take a deep learning-based computer vision approach to leverage the often glaring visual cues exhibited by SE attack campaigns. Additionally, to enable a practical deployment on devices with a variety of screens and browser window sizes, we design *SENet* to be able to classify images (webpage screenshots) of arbitrary sizes.

2.1. Approach Motivation

At a high level, our approach towards building an SE detection system is informed by the following observations:

SE attacks have a very significant visual component: SE attacks exploit a victim’s decision-making processes by using a number of deception and persuasion tactics. To attract users’ attention and deceive/persuade them of the veracity of an invented scenario (e.g., the user’s device is compromised, a software update is needed to watch a video, etc.), web-based SE attacks make use of strong visual cues, including

fake dialog boxes, abused logos/brands, flashy messages, etc., as shown by the examples in Table 1 and Figure 5. Therefore, our image classification approach aims to detect the visual traits of such attacks.

SE attacks are typically orchestrated via SE campaigns: To scale the attacks and facilitate their distribution to a large number of potential victims, SE attacks are orchestrated via SE campaign. Attack campaigns share some similarities with legitimate advertisement campaigns. In legitimate advertisement, the same product/image (or few image variants) is advertised in multiple venues (either physical or online). Similarly, an SE campaign aims to “advertise” visually similar/same SE attacks on multiple different websites, as also noted in [9]. Thus, it may be sufficient to observe and learn from few examples of an SE campaign to allow us to detect future instances of the same or similar SE attacks on different websites.

Based on the above observations, we build a system that aims to continuously collect examples of in-the-wild SE attacks belonging to a variety of campaigns and train a model that can detect new SE attack variants that share visual traits with previously observed SE campaigns.

2.2. Framework Components

At a high level, the three components of our *SEShield* framework work as follows:

SECrawler: As we aim to learn to automatically identify web-based SE attacks, we first need to be able to continuously collect fresh examples of web pages related to SE attack campaigns. To this end, we reimplement and extend the SE attack discovery approach proposed by Vadrevu et al. [9]. Specifically, we extend [9] by significantly increasing the number of different supported devices and screen resolutions (from 5 to 30) and by keeping track of the path followed by the crawler to reach a potential SE attack page. We then use these improvements over [9] to collect larger and more detailed datasets of SE attack campaigns, which we use for training and evaluating our *SENet* module. Our data collection and systematic labeling process will be presented in Section 3.1.

SENet: The *SENet* module represents the primary contribution and main focus of our research. Using examples of SE attack campaigns collected with our *SECrawler*, as well as negative examples consisting of benign web pages, we train a novel deep learning-based visual SE attack classifier. As mentioned earlier, we aim to deploy our SE attack classifier on a variety of devices, including laptops, desktops, and mobile devices, which can have widely different screen resolutions. Therefore, we want our classifier to support input images (i.e., web page screenshots) of arbitrary sizes. However, this is not always easy to accomplish with traditional convolutional neural networks (e.g., VGG, ResNet, etc.) and training approaches, which are designed to expect images of fixed size in input. To solve this issue, we adapt existing deep learning architectures to build an image classifier that can generalize to classifying web page screenshots of any

screen size with high accuracy. In addition, we design a new distributed learning approach inspired by federated learning to be able to train our model over images of arbitrary sizes with limited GPU resources. We will present the details of the architecture and implementation of *SENet* in Section 3.2.

SEGuard: Once our *SENet* classifier is trained, we demonstrate the practicality of our SE defense framework by developing a prototype Chrome extension that deploys the *SENet* model into the browser. Our browser extension, named *SEGuard*, is programmed to detect SE attacks in near real time. It does so by capturing a screenshot of each webpage on which a meaningful user interaction is observed, such as a mouse click or key press, and by using *SENet* to classify the screenshot image as either *SE attack* or *benign* (i.e., not SE-related). Note that our system could also be integrated natively into the browser’s code, similar to Chrome’s built-in phishing-specific detector [18]. More details on the implementation of *SEGuard* are discussed in Section 3.3.

In the following sections, we describe the components of our system in more detail and present a comprehensive evaluation of the entire *SEShield* framework, with particular focus on measuring the detection performance and generalization abilities of our *SENet* classifier.

3. Framework Details

In this section, we provide more details on each of the components of the *SEShield* framework, with particular focus on *SENet*, which represents our main contribution.

3.1. SECrawler

While research on phishing defenses can leverage URL feeds such as PhishTank [19] and OpenPhish [20] to collect ground truth data, to our best knowledge there exist no analogous feeds or repositories that would allow us to readily collect fresh samples of generic SE attacks. Therefore, we had to build our own system for discovering and collecting recent examples of such attacks in the wild. To this end, we extended the SE attack campaigns discovery approach proposed in [9]. Briefly, the approach is based on a *crawler farm* that is seeded with URLs that are likely to lead to SE attacks. A crawler consists of an instrumented browser that loads a seed URL and automatically interacts with web pages in an attempt to trigger a redirection to an SE attack. A number of heuristics are used to pilot the browser (please refer to [9] for details) to collect *landing pages* that have a high likelihood of being related to SE attacks. As these landing pages are visited, the crawler records the related URL and a screenshot. Then, to discover SE attack campaigns and filter out noise (i.e., non-SE pages), a webpage screenshot clustering algorithm is used, which is based on the intuition that SE attacks are typically orchestrated into SE campaigns that distribute the same (or very similar) attacks across multiple malicious domain names.

To enable our data collection, we reimplemented an instrumented browser similar to the one proposed in [9]

using Puppeteer [21] and extended it to add the following improvements:

Improved crawler heuristics: In [9], “click-worthy” page elements were prioritized by sorting them simply in decreasing element size order (i.e., based solely on the size of an element on the rendered webpage). To allow *SECrawler* to more quickly reach SE attack content, we empirically derived additional heuristics. For instance, we prioritize interacting with page elements (e.g., buttons, images, links, etc.) that include keywords such as *update*, *download*, *play*, etc. (we used a total of 38 keywords often found on pages that lead to SE attacks). This small improvement over [9] allowed our crawler to reach more attacks. Additionally, compared to [9], we added the use of [22] to improve the “stealthiness” of our crawlers (i.e., make it more difficult for pages to detect browser automation) and yield a larger variety of SE attacks.

Improved data granularity: More importantly, compared to [9], we collect finer-grained contextual information around SE attacks with two improvements: (1) We implemented our *SECrawler* to track all steps that a crawler followed to reach a given page, which enables *attack traceback*; (2) Because one of our main goals is to develop a practical defense that can be deployed on devices with widely different screen resolutions, we significantly extended the number of devices and screen sizes emulated by our crawlers, from 5 to 30; To select the screen sizes and devices to be emulated, we relied on external statistics [23] as well as results from a prior IRB-approved user study (from an unrelated research project) involving 400 MTurk.com users that allowed us to derive the most popular viewport sizes and screen aspect ratios to be embedded in our *SECrawler* system.

Systematic labeling process: As in [9], after suspected SE attacks are clustered into potential campaigns and noise is removed using conservative heuristics, there is a need for manual intervention to confirm and label SE attack campaigns. Unlike in [9], we use a systematic labeling approach. Namely, we label potential SE attack campaigns and remove non-SE pages by using three different human labelers with expertise on web security and social engineering attacks who were tasked with labeling each cluster of webpage screenshots as either *SE Campaign* or *benign* (i.e., not SE). After the labelers independently completed their tasks, they met to discuss and attempt to resolve possible label disagreements. In the rare cases in which consensus on the label to be assigned could not be found, they marked the related cluster as *unknown* and excluded it from further consideration. This systematic data labeling process allowed us to collect higher quality SE attack examples. We computed the inter-rater reliability score using Krippendorff’s alpha score [24] among the labelers and obtained $\alpha = 0.82$, which indicates a high level of agreement [25]. Besides collecting and labeling examples of SE attacks, we also used our *SECrawler* to collect benign webpages under 30 different screen resolutions by seeding it with a list of popular websites (the top 600 websites according to Tranco [26]).

3.2. SENet

To provide an effective solution for in-browser detection of generic SE attacks, we need to take into account that web pages can be rendered on devices with widely different screen resolutions or browser windows of arbitrary size. Therefore, unlike traditional image classification models, which are typically trained assuming input images of fixed size, our SE detection system needs to be able to classify images of arbitrary size and generalize to different types of SE attacks.

To build *SENet* in a way that enables it to classify images of arbitrary sizes, we proceed as follows. We start from popular pre-trained deep learning models (e.g., VGG19, ResNet50 Xception, etc.), to take advantage of fine-tuning approaches and avoid having to train a large model from scratch. We adapt the model’s architecture by removing their pre-trained classifier “head” and replacing it with a new binary classification layer. Furthermore, we replace the input layer to remove the hard constraint on the expected size of input images (we set the input height and width to “None”). We then fine-tune the model by training it on our dataset of SE attacks and benign pages. Finally, we compare the performance of different models and choose the model that provides the best trade-off between true and false positives (details are provided in Sections 4.2 and 5).

Some models, such as VGG16, VGG19, etc., include a flattening layer in their classifier “head,” to reshape the output of convolutional layers into a vector that can be used in input to dense layers. However, the flattening layer is expected to produce a fixed size output vector, which is not the case if the input image is not of the specific fixed size expected by the model. Thus, we adapt such models by removing the classifier “head” and flattening layer, and by adding a global pooling layer, whose output size is independent of the input image size. As a concrete example, consider the VGG19 model pretrained on ImageNet [27], which can only accept images of a fixed size 224x224, as shown in Figure 2. The main obstacle to adapting VGG19 to classifying images of arbitrary size is the Flatten layer, which generates a vector of fixed size (25,088 elements), and the subsequent Dense layers. To adapt the model, we remove the last 4 layers, add a global pooling layer, and then include a binary dense layer to predict *SE* vs. *benign* web page screenshots. Finally, we fine tune this new model with training examples of SE attacks and benign web pages.

Notice that, in our case, simply resizing the input images to fit a fixed input size is not a good option. The reason is that, as mentioned earlier, web page screenshots can have widely different sizes, depending on the device and browser in which they render. Thus, resizing an input screenshot can sometimes cause significant distortions, which can make accurate classification difficult. Instead, our approach allows us to keep the aspect ratio of all input web pages intact and at the same time to achieve high classification accuracy.

Also, one may think that we could address the challenges mentioned earlier by building a separate classifier for each of the possible input image sizes. However, this approach

a) Original VGG19 architecture

Layer (type)	Output Shape	Param #
input_1 (InputLayer)	[(None, 224, 224, 3)]	0
block1_conv1 (Conv2D)	(None, 224, 224, 64)	1792
....		
block5_conv4 (Conv2D)	(None, 14, 14, 512)	2359808
block5_pool (MaxPooling2D)	(None, 7, 7, 512)	0
flatten (Flatten)	(None, 25088)	0
fc1 (Dense)	(None, 4096)	102764544
fc2 (Dense)	(None, 4096)	16781312
predictions (Dense)	(None, 1000)	4097000

b) Adapted VGG19 architecture for arbitrary size input images

Layer (type)	Output Shape	Param #
input_1 (InputLayer)	[(None, None, None, 3)]	0
block1_conv1 (Conv2D)	(None, None, None, 64)	1792
....		
block5_conv4 (Conv2D)	(None, None, None, 512)	2359808
block5_pool (MaxPooling2D)	(None, None, None, 512)	0
gmp2d_1 (GlobalMaxPooling2D)	(None, 512)	0
predictions (Dense)	(None, 2)	1026

Figure 2: Original vs. adapted VGG19 architecture.

would incur three major problems: (i) it is difficult to collect a large enough number of training examples for each different screen resolution, (ii) on laptop and desktop devices, the browser window could be set by the user to any arbitrary size and aspect ratio that cannot be easily anticipated, and (iii) training separate classifiers would make it difficult to leverage similarities between web pages (malicious or benign) rendered on different screen sizes. Therefore, we chose to train a single model that leverages training images of many different sizes, which helps us to better generalize to any arbitrary input size at test time.

Model selection process: To find a pre-trained model that performs well on our specific web page classification problem, we adapted (when needed) and compared five different popular models that are characterized by different model complexity (i.e., number of weights) and accuracy. Namely, we fine-tuned and compared VGG-16 and VGG-19 [28], Inception-ResNet-v2 [29], ResNet50V2 [30], and Xception [31], all pre-trained on the ImageNet [32] dataset.

To reduce the amount of compute resources and time needed for the comparison of these five models with multiple combinations of hyperparameters, we trained each of the models on a fixed reduced-size dataset of 500 real-world SE attacks and 500 benign images and tested on 100 benign and 100 SE images. During these preliminary model selection experiments, we found that VGG-19 performed about 20% better than other models in terms of both false positives and false negatives. We therefore selected VGG-19 as the reference model for all subsequent experiments, whose results are reported in Section 5.

Implementation challenges and solutions: One of the main implementation challenges we faced while working with models that support images of arbitrary sizes is related to distributing the training workload. First, our dataset of web page screenshots is too large to fit in a single GPU’s memory (we experimented with 48GB A40 NVIDIA GPUs). Furthermore, while popular deep learning frameworks support distributed training (e.g., Tensorflow [33]), the distributed training APIs typically expect input tensors of consistent,

fixed size. After several unsuccessful attempts to adapt existing frameworks, we then realized that this would be very challenging for a small research team and we then chose to instead build a custom distributed training framework inspired by federated learning [34] that would fit our needs.

Federated learning [34] allows for training a model based on data that is distributed across numerous devices, whereby each device performs local training and only shares model updates with a central server. The central server then aggregates the model updates to obtain a final model. To train *SENet*, we devise an approach inspired by federated learning that we named *localized federated learning*, in which we create a set of virtual devices, or training *clients*, and a training *server*, and assign each client with a different portion of the training dataset. Then, each client trains a model on the data assigned to it and sends the model weights to a the training server, which computes a global trained model. This strategy allows us to avoid loading the entire dataset at once and exhaust the GPU’s memory. Also, it allows us to partition the dataset in small sub-datasets and to assign randomly selected sub-datasets to different clients.

Since each client can train its local model separately from the others, we only need to train the model on a sub-dataset at a time, thus avoiding GPU memory exhaustion problems. Additionally, this makes it easy to scale to multiple GPUs, as different clients can train in parallel on different GPUs. It is also worth noting that each client can train on images of different sizes, which helps with generalization. The only constraint is that training images in a single minibatch must all be of the same size. However, during an epoch each client will be trained on many minibatches belonging to its assigned sub-dataset, with each minibatch being related to a randomly selected set of images all having the same size within that minibatch. Algorithm 1 summarizes the high-level steps involved in training *SENet* using this approach.

3.3. SEGuard

To further demonstrate the practicality of our system, we develop a proof-of-concept extension for the Chrome browser that allows for detecting SE attacks in real time. As the user browses the web, every time a new URL is visited, the extension waits to check if the user interacts with the page (e.g., via mouse click). Then, if an interaction occurred, it takes a screenshot and passes the related image to the *SENet* classifier to determine if the visited page contains an SE attack, and if so it presents the user with an alert.

More precisely, *SEGuard* takes the following steps. (i) When a new page is visited, we can first check if the associated domain name is present in an allowlist (e.g., a list of the top most popular websites according to Tranco [26]), in which case no action is taken. (ii) If the page is not in the allowlist, *SEGuard* waits for a meaningful user interaction with the page, such as a *click*, *keypress*, etc., event. If one of such events occurs, a screenshot of the browser viewport is captured. Waiting for a meaningful user interaction with the page is motivated by the fact that, unlike drive-by browser

Algorithm 1 Training *SENet* with localized federated learning

Input:

M : VGG19 pre-trained on Imagenet
 GE : Global epochs
 CE : Client epochs
 CC : Client count
 SW : List of client weights

Output: A fine-tuned VGG19 model

```
1: for all  $j = 1$  to  $GE$  do
2:   for all  $i = 1$  to  $CC$  do
3:     Set  $clientModel.weights = M.weights$ 
4:     Assign dataset partition to the  $i$ th client
5:     Group images in  $i$ th dataset partition into minibatches
      based on image size
6:     Train the  $clientModel$  for  $CE$  epochs
7:     Scale the weights of  $clientModel$  based on  $CC$ 
8:      $SW.insert(clientModel.weights)$ 
9:   end for
10:  Set  $averageWeights =$  average of weights in  $SW$ 
11:  Set  $M.weights = averageWeights$ 
12:  Evaluate  $M$  on validation data
13: end for
```

exploits, SE attacks often require the user to interact with the page to click on a button, click on a (fake) notification, etc., for the attack to succeed (notice that other heuristics may also be used to determine if/when to take a screenshot). (iii) Once a screenshot is taken, we feed into our *SENet* model, and if it is classified as an SE attack the user is informed via an alert drawn over the page by the extension.

As mentioned earlier, to classify a page we leverage *SENet*'s deep learning model. However, we first need to adapt *SENet* to be used within a browser extension. Thus, we first converted the *SENet*'s model using the TensorFlowJS [17] tool set. One important factor in implementing *SEGuard* is performance, especially in terms of classification latency. Initially, we translated *SENet*'s VGG-19 based model, which we found to have the best detection accuracy (see Section 4.2). Unfortunately, large models such as VGG-19 tend to have poor performance during inference on regular devices (e.g., a normal laptop) without GPU or other high-performance hardware. To reduce the latency related to obtaining the classification decision for a given webpage screenshot, we therefore implemented a more light-weight version of *SENet* based on the MobileNet [35] architecture, which provided significant latency reduction with a limited impact on accuracy. We will present more details on *SEGuard*'s evaluation with both models in Sections 4.3 and 5.5.

4. Experimental Setup

In this section, we discuss how we setup the *SEShield* framework's modules to enable our evaluation.

4.1. *SECrawler* Setup

Our goal is to supply *SECrawler*'s browser farm with seed URLs that are likely to lead to SE attack web pages. To this end, we use the following setup.

Environment Setup: We use Docker to run many parallel instances of *SECrawler*'s instrumented browser. Each instance represents an isolated and clean environment that does not retain any session information related to crawling previous seed URLs. We deploy our crawlers on a server with 24 CPU cores running Ubuntu Linux, where we run 15 crawler instances at a time. For any given seed URL, we visit it using multiple instances of our instrumented browser, each configured so to emulate one of 10 different browser/device combinations, including different smartphones, tablets, laptops, etc., and browsers that render pages with different viewport sizes (the browser/OS combinations we use include Firefox on Windows, Safari on Mac, Edge on Windows, Chrome on Windows, Chrome on Linux, Chrome on Mac, Chrome on an Android Phone, Safari on iPhone, Safari on iPad, and Chrome on different Android tablets). Additionally, to make our crawling as stealthy as possible and make the anti-crawler mechanisms implemented by some ad networks more difficult, we used Puppeteer's "stealth" libraries [36].

SE Seed URLs: To collect seed URLs that may provide a high-yield of SE attacks, we follow an approach similar to previous studies [9], [10] and collect URLs of websites that are known to host ads from low-tier ad networks, as they have been observed to often lead to SE attack pages. We compiled a list of such ad networks and leveraged PublicWWW [37], a reverse code search engine, to find URLs of websites that contained code-related keywords associated with each ad network. Overall, we collected a total of 24,979 seed URLs associated with 10 low-tier ad networks (listed in Table 11, in Appendix).

SE Attacks Collection: By visiting the seed URLs, our crawlers collected web pages related to 55,539 distinct URLs and took 650,255 distinct screenshots. Notice that *SECrawler* takes multiple screenshots per pages, for instance right before the crawler interacts with the page (e.g., click on an element), for every newly opened tabs resulting from the interaction, and in case of changes in the HTML of the current visited page that result from an interaction. In addition, to increase dataset diversity, we also added 28,923 screenshots provided to us by the authors of [9], for a total of 679,178 images. We further process the screenshots to remove duplicates, and cluster images based on their resolution and by using an image similarity metric based on perceptual hashing, similar to previous work [9], [13]. After filtering, we were left with 8,107 images in 318 clusters that needed to be labeled. To label these image clusters, we relied on a systematic manual labeling process with three expert labelers per image (as described in Section 3) to identify SE attack campaigns with high-confidence ground truth labels. As a result, we found 258 clusters of SE attack pages. Overall, these clusters consisted of 7,484 images related to 30 different screen resolutions. By

further (manually) grouping the 258 image clusters related to different resolutions into meta-clusters based on attack type similarity, we obtained 74 different SE attack *campaigns*. This new dataset is summarized in Table 2, where we also contrast ours with the dataset provided by [9]. Table 12 (in Appendix) reports a more detailed dataset composition breakdown, whereas Table 3 summarizes the number of SE campaigns and different screen resolutions per each attack category (e.g., notification stealing, scareware, etc.).

TABLE 2: Overview of SE attacks dataset.

Dataset	Campaigns	Screen Resolutions	Screenshots
New data	30	28	2,490
[9]	44	3	4,994
Total	74	30 (1 common res.)	7,484

TABLE 3: SE attack categories represented in our dataset and number of campaigns and different screen resolutions of web page screenshots we collected.

Attack Category	# of Resolutions	# of Campaigns
Fake Software Download	27	29
Notification Stealing	26	7
Service Sign-up Scam	24	20
Scareware	11	9
Fake Lottery/Sweepstakes	4	6
Technical Support Scam	2	3

Benign Webpage Collection: To collect examples of benign (i.e., non-SE) web pages, we rely on Tranco [26] and select seed URLs for domains with $\text{rank} \leq 5,000$. Overall, we collected 396,255 distinct screenshots by navigating through multiple pages on popular websites using different (emulated) devices and screen resolutions, as for the SE attacks collection.

4.2. SENet Setup

As we mentioned in Section 3.2, after conducting preliminary model selection experiments by comparing five different pretrained models with different architectures, we determine that VGG19 performed the best among them. We therefore used VGG19 pre-trained on ImageNet to build *SENet*. To perform all *SENet* experiments, we used a dedicated Dell PowerEdge R750xa server with 256GB memory and two 48GB NVIDIA A40 GPUs running CUDA 11.8 and TensorFlow v2.8.4.

4.2.1. Hyperparameter Tuning. Before training the full *SENet* model, we performed numerous systematic experiments using a reduced dataset of 500 real-world SE attacks and 500 benign training images and 100 benign and 100 SE test images to tune the model’s hyperparameters so to extract the best performance results on a validation dataset. We used the Adam optimizer with an initial learning rate of $1E-3$, and then tested both lower and higher learning rates.

Concurrently, we unfroze either all or a subset of VGG19’s `block5` and `block4` convolutional layers. Through these experiments we explored the combination of different learning rate and different unfrozen layers and discovered that setting the learning rate $1E-5$ and unfreezing only the `block5` convolutional layers yielded the best outcomes for our *SENet* classifier.

Because some of the web page screenshots are quite large (e.g., when taken on a 1920x1080 screen resolution), we reduce input images by using a scaling factor while maintaining the same width/high ratio. After systematically experimenting with different values of s ranging from 2 to 8, we found that using $s = 4$ for desktop and laptop screen resolutions and $s = 2$ for mobile device resolutions (i.e., smartphone and tablet) gave us an optimal trade-off between training time and detection accuracy.

After hyperparameter tuning, we conducted different experiments using the full dataset (see Table 2) and our localized federated learning algorithm described in Section 3.2 (Algorithm 1). While the composition of the training and test dataset changed depending on the experiment (see details in Section 5), our models were trained using a consistent setup across all evaluation scenarios during the training process. First, in each case we applied data augmentation to the training images and formed a training dataset containing 15,000 benign images and 15,000 SEA images, with approximately 500 images per each of the 30 resolutions represented in our overall dataset. For the localized federated learning algorithm described in Section 3.2 (Algorithm 1), we found that using $CC = 5$ clients with training epochs $CE = 5$ gave us the best results, while the server’s maximum training epochs was set to $GE = 50$, with a batch size of 32. During our experiments, we saved a model checkpoint at every 5 epochs and saved the results for the best performing model checkpoint on the testing dataset.

4.2.2. Data Augmentation. To augment the training dataset, we performed data augmentations to increase the deep learning model’s generalization power. Given the training dataset, for each screen resolution we randomly select images (i.e., screenshots) to which we apply a randomly chosen augmentation algorithm among the ones listed below. Because of the nature of the webpage content, we made sure not to corrupt either the readability of the text content or the orientation of the webpage object, when we chose the augmentation functions. We apply random parameters (e.g., brightness level, crop size and crop windows position, etc.) for each image augmentation, to reduce the possibility of obtaining duplicate images. Every image undergoes the following image augmentations: color inversion, gray scaling, random margin cropping, huge level change, saturation, contrast, brightness, and solarization. The goal is to help the model avoid focusing on specific page artifacts, such as specific colors or the exact page size and size of the page margins, which can in turn help prevent shortcut issues related to shortcut learning [38].

4.3. *SEGuard* Setup

To build *SEGuard*, we implemented a proof-of-concept Chrome browser extension that embeds our *SENet* classifier. As mentioned earlier, we initially embedded *SENet* in the extension by translating the VGG19 model to JavaScript (JS) using the TensorFlowJS framework. However, we quickly realized that the inference time was too large, in the orders of a few seconds, and did not meet our near real-time classification goals. Considering that the *SENet* model based on VGG19 is quite large, with a parameter count of 144 million, it is not a suitable model for implementation in a browser extension. Therefore, we trained a more lightweight version of *SENet* based on MobileNetV2 [35]. To this end, we used MobileNetV2 pre-trained on ImageNet and followed a process similar to what described in Section 3.2. In terms of detection performance on ImageNet, MobileNetV2 is quite comparable to VGG19, as both models achieved a top-1 accuracy of 71.3% on the ImageNet validation datasets [39]. Because MobileNetV2 expects input images of fixed size, we had to modify its architecture to accommodate the classification of images of arbitrary sizes (similar to what we explained in Section 3.2). We then fine-tuned the model and translated it using TensorFlowJS to embed it in our proof-of-concept extension. With this approach, we were able to reduce inference time by more than an order of magnitude while maintaining high accuracy. We provide more details on the evaluation of *SEGuard* in Section 5.

5. Experimental Results

We evaluated *SENet* to answer a number of research questions (RQs), as indicated in the following subsections. For instance, we evaluated whether *SENet* can detect new instances (i.e., new SE attack pages) of previously observed attack campaigns, generalize to previously unseen screen resolutions, detect instances of never-before-seen campaigns, etc.

Please notice that in all tables reported below, “DR at 1% FP” indicates the detection rate at a 1% false positive rate, whereas F1, Precision, Recall and Confusion Matrix are computed at the default 0.5 detection threshold.

5.1. *SENet* Detection Results

RQ1: Can *SENet* accurately identify *new* instances of SE attacks belonging to previously observed campaigns?

To answer this question, we evaluate the detection capabilities of our *SENet* model on randomly chosen test data. To this end, we randomly select 500 benign examples and 500 SE attacks, which are kept separate from the training dataset. Notice that the related web page screenshots were selected across randomly chosen screen sizes and SE attack campaigns. To compose the training dataset, we proceeded

as indicated in Section 4.2. The results are reported in Table 4, and the (zoomed in) Receiver Operating Characteristic (ROC) curve in Figure 3. In this setting, *SENet* achieves a detection rate of 99.6% at 1% false positives.

TABLE 4: *SENet*’s detection results.

F1	Recall	Precision	Accuracy	Confusion Matrix	AUC	DR at 1% FP
0.994	0.992	0.996	0.994	TN: 498 FN: 4 FP: 2 TP: 496	0.999	0.996

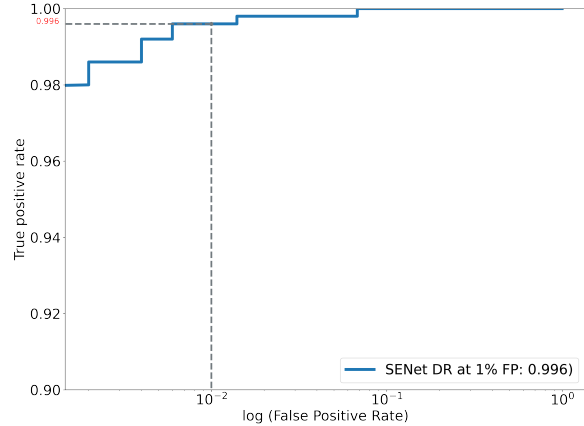


Figure 3: ROC curve for the VGG-19-based *SENet* model.

5.2. Generalization to Never-Before-Seen Screen Sizes

RQ2: Can *SENet* accurately identify *new* instances of SE attacks captured on a screen size never seen during training?

To answer RQ2, we proceeded as follows. First, we selected 9 different screen resolutions from our dataset. Among these 9 resolutions, 5 are landscape resolutions while the other 4 are portrait resolutions related to mobile devices. Let r_i indicate one of these 9 resolutions. Then, we formed 9 different training datasets, $\{T_1, \dots, T_9\}$, where dataset T_i was formed by selecting images from all resolutions except for r_i . The remaining images with resolution r_i were set aside as test dataset S_i . We then performed 9 training/test experiment by training on T_i and testing on S_i (i.e., images with the excluded resolution r_i). Notice that, because *SECrawler* visits the same URLs using different browser viewport sizes, the same SE attack campaigns can typically be observed under different resolutions. Therefore, T_i and S_i can include common instances of benign pages and SE attacks from the same campaigns, but the training and test images have different sizes. This allows us to focus on the effect of web page screenshots taken on never-before-seen screen sizes, rather than the effects of previously

unseen benign pages or SE attack campaigns. Also, to obtain a roughly balanced test dataset, where a particular SE attack campaign does not dominate the others, given resolution r_i we selected at most 10 images from each SE attack campaign represented under that resolution and 1,000 random images from benign pages in the same resolution.

The results of this experiment are reported in Table 5 and in Figure 4. “Global” refers to the overall results computed by first combining the classification scores obtained during the 9 training/test experiments into a single scores set. It is notable that *SENet* can generalize very well to previously unseen resolutions, with detection rates above 95% at 1% false positives. A partial exception (88% detection rate) is represented by 360x640, which is typical of older or low-end smartphones. We hypothesize this is due to the particularly small size of this screen resolution, compared to modern devices (notice that the F1, Precision, and Recall values in the table are computed at the default 0.5 detection threshold, rather than the tuned thresholds that would be used in operation to stay below 1% FPS).

TABLE 5: Results for generalization to new screen sizes. “DR at 1% FP” indicates the detection rate at a 1% false positive rate. F1, Precision, Recall and Confusion Matrix are instead computed at the default 0.5 detection threshold.

Test Res.	F1	Recall	Precision	Accuracy	Confusion Matrix	AUC	DR at 1% FP
800x1280	0.795	1.0	0.66	0.984	TN:983 FN: 0 FP:17 TP:33	0.998	1.0
414x896	0.645	1.0	0.476	0.99	TN:989 FN: 0 FP:11 TP: 10	1.0	1.0
768x1024	0.565	1.0	0.394	0.98	TN:980 FN: 0 FP:20 TP:13	0.997	1.0
360x640	0.825	0.94	0.734	0.981	TN:983 FN: 3 FP:17 TP:47	0.992	0.88
1366x768	0.94	1.0	0.887	0.994	TN:994 FN: 0 FP:6 TP:47	0.999	1.0
1920x998	0.943	1.0	0.892	0.996	TN:996 FN: 0 FP:4 TP:33	0.999	1.0
1478x837	0.941	1.0	0.889	0.995	TN:753 FN: 0 FP:4 TP:32	0.999	1.0
1536x824	0.976	0.959	0.993	0.994	TN:999 FN:6 FP:1 TP:140	0.998	0.959
1366x728	0.98	0.984	0.977	0.996	TN:997 FN:2 FP:3 TP:125	0.999	0.984
Global	0.911	0.978	0.853	0.99	TN: 8674 FN:11 FP: 83 TP:480	0.997	0.978

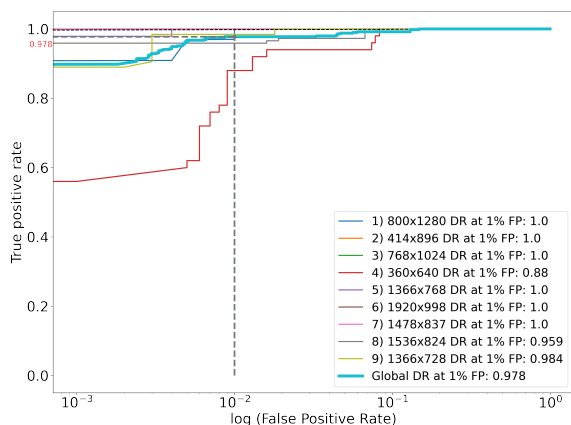


Figure 4: ROC curve for the generalization to new screen sizes. Notice that false positives are represented in logarithmic scale, to highlight the classifier’s performance at low false positive rates.

5.3. Generalization to Never-Before-Seen SE Attack Campaigns

RQ3: Can *SENet* identify web pages belonging to never-before-seen SE attack campaigns?

To test whether our model is able to generalize to detecting SE attack pages related to never-before-seen SE attack campaigns, we performed the following experiments.

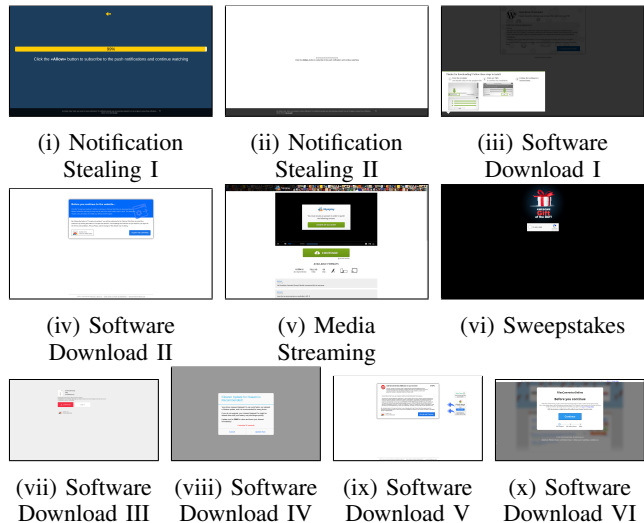


Figure 5: Examples of screenshots from each of the 10 randomly selected test campaigns.

To setup this experiment, we first randomly selected 10 SEA campaigns, $\{c_1, \dots, c_{10}\}$, to be excluded (in turn) from training and used for testing. Additionally, we randomly selected 5000 benign pages from randomly chosen screen resolutions. Example screenshots (one per campaign) for the 10 campaigns $\{c_1, \dots, c_{10}\}$ are shown in Figure 5. Notice that while popular SE attack categories, such as Software Download and Notification Stealing are (by chance) represented multiple times, the specific campaigns within those categories are different (e.g., different fake software being distributed and different visual appearance of the attack page). We then trained 10 models, $\{T_1, \dots, T_{10}\}$. For each model, T_i , we excluded one SEA campaign, c_i , and 500 randomly chosen benign images from training. We then tested the model on the excluded SE campaign and benign images.

The results of this experiment are reported in Table 6 and in Figure 6. We can see that *SENet* is able to generalize well to never-before-seen attack campaigns, with a detection rate of 92% at 1% false positives for all test campaigns but one, namely Campaign 2. An example screenshot for Campaign 2 is shown in Figure 5ii. This is a notification stealing SE attack that shows an almost entirely blank page, which makes it difficult for our classifier to identify significant visual traits that are typical of other campaigns.

Nonetheless, more than about 70% of SE attack page screenshots belonging to this campaign can still be detected by *SENet* at 1% false positives.

TABLE 6: Results for the generalization to never-before-seen SE campaigns.

Model name	F1	Recall	Precision	Accuracy	Confusion Matrix	AUC	DR at 1% FP
Campaign 1	0.897	0.827	0.979	0.966	TN: 498 FN: 19 FP: 2 TP: 91	0.997	0.973
Campaign 2	0.297	0.183	0.786	0.907	TN: 497 FN: 49 FP: 3 TP: 11	0.992	0.87
Campaign 3	0.959	1.0	0.921	0.991	TN: 495 FN: 0 FP: 5 TP: 58	0.998	1.0
Campaign 4	0.971	1.0	0.944	0.993	TN: 496 FN: 0 FP: 4 TP: 67	1.0	1.0
Campaign 5	0.952	1.0	0.909	0.994	TN: 497 FN: 0 FP: 3 TP: 30	0.998	1.0
Campaign 6	0.833	1.0	0.714	0.988	TN: 494 FN: 0 FP: 6 TP: 15	0.996	1.0
Campaign 7	0.966	1.0	0.935	0.995	TN: 497 FN: 0 FP: 3 TP: 43	0.999	1.0
Campaign 8	0.909	1.0	0.833	0.989	TN: 494 FN: 0 FP: 6 TP: 30	0.997	1.0
Campaign 9	0.99	1.0	0.98	0.997	TN: 498 FN: 0 FP: 2 TP: 96	0.999	1.0
Campaign 10	1.0	1.0	1.0	1.0	TN: 500 FN: 0 FP: 0 TP: 88	1.0	1.0
Global	0.912	0.886	0.94	0.982	TN: 4966 FN: 68 FP: 34 TP: 529	0.997	0.925

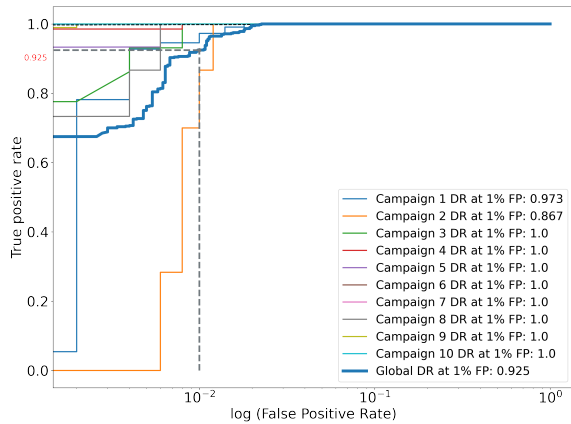


Figure 6: ROC Curve for Generalization to Never-Before-Seen SE Campaigns on Single Dataset

5.4. Adversarial Examples Evaluation

RQ4: Can *SENet* be strengthened against adversarial examples?

Because SE attack pages are under the attacker’s control, the attacker can attempt to craft attack pages that explicitly attempt to evade *SENet* by injecting adversarial noise. At the same time, attackers must operate under two concurrent constraints: (i) SE attack pages must maintain their visual attack components, and (ii) the level of injected noise should be limited so not be noticeable to users.

It is well known that adversarial examples forged by adding small perturbations can reduce deep learning models’ classification accuracy [40] and that adversarial training is an effective approach to make models (at least partially) more robust to them [41]. In this section, we first test *SENet* against white-box adversarial attacks, and then show that adversarial training can significantly increase its robustness to such attacks. To this end, we follow advice provided by highly cited previous work in this area [42] and use

projected gradient descent (PGD) to construct adversarial images in a white-box attack setting using the Foolbox library [43], [44]. The level of perturbation is controlled by the ϵ parameter. The higher the value of ϵ , the more noticeable the perturbation to the human eye. At the same time, larger ϵ values increase the likelihood of evading a deep learning model. Therefore, we experimented with increasing values of ϵ , starting from 0.01. As shown in Figure 7, as ϵ reaches 1 the noise becomes very noticeable.



Figure 7: Adversarial Examples Generated with PGD

TABLE 7: Results for different PGD ϵ values.

ϵ	F1	Recall	Precision	Accuracy	Conf. Matrix	DR at 1% FP
NONE	0.994	0.992	0.996	0.9936	TN: 433 FN: 4 FP: 2 TP: 496	0.996
0.01	0.993	0.99	0.996	0.9925	TN: 433 FN: 5 FP: 2 TP: 495	0.996
0.1	0.99	0.984	0.996	0.9893	TN: 433 FN: 8 FP: 2 TP: 492	0.988
0.3	0.8732	0.778	0.9949	0.8791	TN: 433 FN: 111 FP: 2 TP: 389	0.8
0.5	0.7145	0.558	0.9929	0.7615	TN: 433 FN: 221 FP: 2 TP: 279	0.616
1	0.4139	0.262	0.985	0.6032	TN: 433 FN: 369 FP: 2 TP: 131	0.27
2	0.4089	0.258	0.9847	0.6011	TN: 433 FN: 371 FP: 2 TP: 129	0.258
3	0.4114	0.26	0.9848	0.6021	TN: 433 FN: 370 FP: 2 TP: 130	0.26
4	0.4038	0.254	0.9845	0.5989	TN: 433 FN: 373 FP: 2 TP: 127	0.254
5	0.4089	0.258	0.9847	0.6011	TN: 433 FN: 371 FP: 2 TP: 129	0.258
8	0.4063	0.256	0.9846	0.6	TN: 433 FN: 372 FP: 2 TP: 128	0.256

Table 7 shows the results of testing our *SENet* using the same setting described in Section 5.1 on adversarial examples constructed with PGD at different values of ϵ . We can see that the detection rate at 1% false positive rate decreases sharply as ϵ grows above 0.3. At 0.5, a user may miss to notice the perturbation but the detection rate decreases to only 0.616.

Adversarial Training: To make our model more robust to adversarial examples, we follow recommendations from previous work [42]. In practice, starting from images in the training dataset, we generate a large number of adversarial examples using PGD with different values of ϵ (specifically, 0.3, 0.5 and 1). Then, during training, we select a random amount of samples to inject into each training batch. For testing, we start from the test dataset and generate adversarial page screenshots. We then tested *SENet* against these adversarial examples. The results are reported in Table 8 and Figure 8. As expected, the model becomes significantly more robust to attacks, even at $\epsilon = 1$, with a detection rate above 97% at 1% false positives.

To further test the performance of our model on never-before-seen SE attack campaigns, we adversarially trained our model and tested it on never-before-seen attack campaigns, in a way similar to the the experiments reported in

TABLE 8: Results after adversarial training.

ϵ	F1	Recall	Precision	Accuracy	Confusion Matrix	DR at 1% FP
NONE	0.994	0.992	0.996	0.9936	TN: 433 FN: 4 FP: 2 TP: 496	0.996
0.01	0.992	0.99	0.994	0.9914	TN: 432 FN: 5 FP: 3 TP: 495	0.99
0.1	0.989	0.986	0.992	0.9882	TN: 431 FN: 7 FP: 4 TP: 493	0.986
0.3	0.9829	0.974	0.9919	0.9818	TN: 431 FN: 13 FP: 4 TP: 487	0.976
0.5	0.9838	0.974	0.9939	0.9829	TN: 432 FN: 13 FP: 3 TP: 487	0.974
1	0.9808	0.97	0.9918	0.9797	TN: 431 FN: 15 FP: 4 TP: 485	0.972

Section 5.3. Notice that the model did not see examples (adversarial or not) from those attack campaigns during training. Below, we report results for two campaigns, namely *Campaign 4* and *Campaign 10*. The results of these new experiments can be seen in Table 9 and Table 10. We can see that even in this more difficult case, adversarial examples from the two campaigns can be identified with $\approx 90\%$ detection rate event at $\epsilon = 1$, for which perturbations are clearly noticeable by humans, and with a detection rate of more than 95% for lower values of ϵ , for which visual perturbations are more subtle.

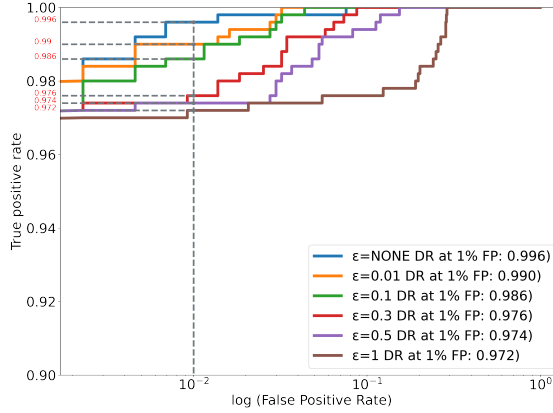


Figure 8: ROC Curve for adversarially trained model.

TABLE 9: Results after adversarial training when SE *Campaign 4* is excluded from training and used for testing

ϵ	F1	Recall	Precision	Accuracy	Conf. Matrix	DR at 1% FP
NONE	0.9504	1.0	0.9054	0.9877	TN: 493 FN: 0 FP: 7 TP: 67	1.0
0.01	0.9504	1.0	0.9054	0.9877	TN: 493 FN: 0 FP: 7 TP: 67	1.0
0.1	0.9504	1.0	0.9054	0.9877	TN: 493 FN: 0 FP: 7 TP: 67	1.0
0.3	0.9504	1.0	0.9054	0.9877	TN: 493 FN: 0 FP: 7 TP: 67	0.985
0.5	0.9429	0.9851	0.9041	0.9859	TN: 493 FN: 1 FP: 7 TP: 66	0.955
1	0.9037	0.9104	0.8971	0.9771	TN: 493 FN: 6 FP: 7 TP: 61	0.896

TABLE 10: Results after adversarial training when SE *Campaign 10* is excluded from training and used for testing

ϵ	F1	Recall	Precision	Accuracy	Conf. Matrix	DR at 1% FP
NONE	0.9832	1.0	0.967	0.9949	TN: 497 FN: 0 FP: 3 TP: 88	1.0
0.01	0.9832	1.0	0.967	0.9949	TN: 497 FN: 0 FP: 3 TP: 88	1.0
0.1	0.9832	1.0	0.967	0.9949	TN: 497 FN: 0 FP: 3 TP: 88	1.0
0.3	0.9659	0.9659	0.9659	0.9898	TN: 497 FN: 3 FP: 3 TP: 85	1.0
0.5	0.9718	0.9773	0.9663	0.9915	TN: 497 FN: 2 FP: 3 TP: 86	0.989
1	0.9101	0.8636	0.962	0.9745	TN: 497 FN: 12 FP: 3 TP: 76	0.909

Overall, these results show that our model can be made more robust via adversarial training, even at high value of ϵ

for which noise is visually noticeable and can therefore tip off the user. While we observed a slight decrease in detection rate, compared to non-adversarial test screenshots, the model still maintains a high level of accuracy and robustness to adversarial manipulations.

5.5. *SEGuard* Evaluation

As mentioned in Section 4.3, VGG19 is too large of a model to be embedded into a browser extension. The main issue is represented by inference latency, which we measured at around 5 seconds per each screenshot classification. This is mostly due to the translation of the model to TensorFlow.js [45] and to the large number of model parameters ($\approx 144M$).

Unfortunately, this high inference latency is not practical for in-browser classification and for alerting the user in a timely manner. Therefore, we decided to experiment with MobileNetV2, a popular lightweight deep learning model [35]. To this end, we trained and evaluated the new model following the same setup for the VGG19 experiments we previously reported in Section 5.2. As shown in Figure 9, MobileNetV2 perform comparably to VGG19 on our dataset, albeit with a lower detection rate at low false positive rates. For instance, at 1% false positives both models successfully detected 90% or more of the SE attack pages, with VGG19 outperforming MobileNetV2 by 7.8%. At the same time, *SEGuard* with MobileNetV2 is able to capture, classify a page, and alert the user within $\approx 200ms$. This significant reduction in latency, compared to VGG19’s 5 second latency, makes in-browser SE defense more practical.

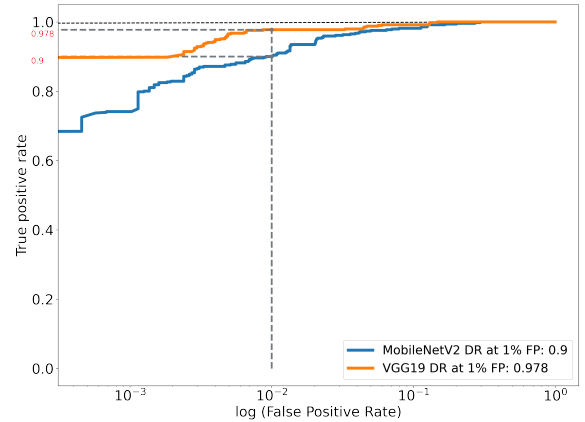


Figure 9: ROC curve for MobileNetV2 vs. VGG-19

6. Discussion and Limitations

In this section, we discuss additional considerations and limitations of our framework.

Privacy-Aware Implementation. As explained in Section 3.3, we implemented *SEGuard* as a self-contained in-browser detection module by “embedding” the *SENet* model into a browser extension. To this end, we had to translate *SENet* into a light-weight model using MobileNet. This *local detection* solution is in contrast with possible alternatives based on API calls to a remote cloud-based service that can run much larger models. However, API-based detection system pose privacy risks, in that they may leak both URLs and webpage screenshots that require classification. Also, passing screenshot over the network to the API may incur significant latency. While some solutions based on locality-preserving image hashing may help to reduce privacy risks, utility and accuracy may be significantly diminished, compared to a local model.

Ethical considerations. Our *SECrawler* follows an approach for collecting SE attacks that was previously proposed in recent research [9], [10], [13], [46] that studied attacks delivered via malicious ads. Similar to previous works, the impact of our crawler experiments on legitimate advertisers is negligible (only few USD at most). At the same time, *SECrawler* allowed us to collect a large dataset of in-the-wild SE attacks and build a novel and effective in-browser defense.

Limitations. While on average our model is able to generalize very well to never-before-seen screen resolutions (see Section 5.2), with a global average of 97.8% detection rate at 1% false positive, we noticed that the performance dropped when encountering images captured at devices of smaller resolutions, such as 360x640 (see ROC curve in Figure 4). This is the smallest resolution we tested on, which is very uncommon on modern smartphone devices¹. The lower performance is likely due to the fact that the input images are scaled down and the web pages can render differently on such small screens. With additional training examples collected for small screen sizes, it may be possible to further improve performance. We leave the study of this corner case to future work.

Also, while our system generalizes well to most never-before-seen campaigns (see Section 5.3), our system may naturally struggle to detect entirely new SE attack campaigns that do not resemble anything that has ever been observed before, or in those cases in which the attack pages contain very minimal visual content (e.g., almost entirely blank pages with little text), as in the case of some notification stealing campaigns. However, it should be noticed that the vast majority of SE attack campaigns do need to include glaring visual content, to attract potential victims, and that while new campaigns and attack instances may differ from previously observed ones, they do often follow a theme and thus some resemblance with past campaigns samples, as also observed in a previous measurement study [9].

Another concern is due to the fact that we train our *SENet* classified based on in-the-wild SE attacks collected by *SECrawler*. This in-the-wild data collection approach may open our system to potential data poisoning attacks.

1. <https://gs.statcounter.com/screen-resolution-stats/mobile/worldwide>

For instance, attackers may try to modify their attack pages to mislead *SENet* when making decision at test time. This may require a more careful manual vetting and labeling of the data, as well as the use of measures to detect poisoning [47] and mitigate its effects on the model [48], [49].

7. Related Works

Most previous research on SE attacks focuses on specific categories of social engineering. For instance, Miramirkhani et al. [4] performed an analysis of Technical Support Scams and reported websites and phone numbers used by scammers. Stone-Gross et al. [3] showed how victims could be deceived to install fake anti-virus programs by employing scareware SE attacks. Kharraz et al. [5] employed a machine learning model to detect online survey scams that led victims to reveal personal information for fake prizes or content. Our work is different because we focus on detecting an effective and practical in-browser system for detecting generic SE attack pages.

Other studies have focused primarily on identifying and measuring the occurrence of social engineering attack campaigns, without offering a detection solution. For instance, Subramani et al. [10] proposed a system called PushAdMiner to collect and discover web push notification messages that can deliver social malicious ad campaigns, whereas Vadrevu et al. [9] introduced a measurement system that automatically collects examples of SE attacks and identifies previously unknown ad networks that promote SE attack campaigns.

Recently, Yang et al. [13] proposed a first approach towards detecting and blocking generic web-based SE attacks in the browser. The proposed system, named TRIDENT, primarily targets SE ads injected into publishers’ webpages by low-reputation ad networks. SE ads are non-traditional ads that themselves utilize social engineering techniques, such as transparent overlays that perform clickjacking. TRIDENT is able *indirectly* detect SE attacks by identifying SE ads. However, not all SE attacks are distributed via SE ads. Unlike [13], our framework directly aims at detecting SE attacks and by recognizing their visual traits.

There is also a large body of research that focuses on detecting phishing attacks. While Phishing can be considered as a subclass of Social Engineering [50], it is characterized by different visual traits and attack mechanisms, as we discussed in Section 1. Recent research has focused on detecting Phishing websites using visual cues. For instance, Abdelnabi et al. [14] used triplet convolutional networks to detect phishing pages by visual similarity. Lin et al. [15] detect Phishing pages by visually detecting abused company logos. Liu et al [16] presented a technique that is a combination of machine learning and browser instrumentation to detect a phishing page by not only using visual cues but also discovering the intention of a phishing webpage that perform credential stealing via web forms. Unlike the above solutions, our system is able to detect generic SE attacks beyond phishing, even if no specific benign website/logo is abused or in absence of credential stealing attempts.

8. Conclusion

We presented *SEShield*, a framework for in-browser detection of social engineering attacks. *SEShield* consists of three main components: (i) a custom security crawler, called *SECrawler*, that is dedicated to scouting the web to collect examples of in-the-wild SE attacks; (ii) *SENet*, a deep learning-based image classifier trained on data collected by *SECrawler* that aims to detect the often glaring visual traits of SE attack pages; and (iii) *SEGuard*, a proof-of-concept extension that embeds *SENet* into the web browser and enables real-time SE attack detection. We performed an extensive evaluation of our system and showed that *SENet* is able to detect new instances of SE attacks with a detection rate of up to 99.6% at 1% false positive, and that is able to detect previously unseen SE attack campaigns.

References

- [1] I. Mann, *Hacking the Human: Social Engineering Techniques and Security Countermeasures*. Ashgate Publishing, Limited, 2008. [Online]. Available: <https://books.google.com/books?id=1veE2f9rPOgC>
- [2] K. Krombholz, H. Hobel, M. Huber, and E. Weippl, "Advanced social engineering attacks," *Journal of Information Security and Applications*, vol. 22, pp. 113–122, 2015, special Issue on Security of Information and Networks. [Online]. Available: <http://www.sciencedirect.com/science/article/pii/S2214212614001343>
- [3] B. Stone-Gross, R. Abman, R. A. Kemmerer, C. Kruegel, D. G. Steigerwald, and G. Vigna, "The underground economy of fake antivirus software," in *Economics of Information Security and Privacy III*, B. Schneier, Ed. New York, NY: Springer New York, 2013, pp. 55–78.
- [4] N. Miramirkhani, O. Starov, and N. Nikiforakis, "Dial One for Scam: A Large-Scale Analysis of Technical Support Scams," in *Proceedings of the 24th Network and Distributed System Security Symposium (NDSS)*, 2017.
- [5] A. Kharraz, W. K. Robertson, and E. Kirda, "Surveylance: Automatically detecting online survey scams," in *2018 IEEE Symposium on Security and Privacy, SP 2018, Proceedings, 21-23 May 2018, San Francisco, California, USA*, 2018, pp. 70–86. [Online]. Available: <https://doi.org/10.1109/SP.2018.00044>
- [6] J. W. Clark and D. McCoy, "There are no free iPads: An analysis of survey scams as a business," in *6th USENIX Workshop on Large-Scale Exploits and Emergent Threats (LEET 13)*, 2013.
- [7] "New data shows ftc received 2.2 million fraud reports from consumers in 2020," <https://www.ftc.gov/news-events/press-releases/2021/02/new-data-shows-ftc-received-2-2-million-fraud-reports-consumers>.
- [8] M. Khonji, Y. Iraqi, and A. Jones, "Phishing detection: A literature survey," *IEEE Communications Surveys Tutorials*, vol. 15, no. 4, pp. 2091–2121, Fourth 2013.
- [9] P. Vadrevu and Roberto Perdisci, "What you see is NOT what you get: Discovering and tracking social engineering ad campaigns," in *Proceedings of the ACM Internet Measurement Conference*, ser. IMC, 2019.
- [10] K. Subramani, X. Yuan, O. Setayeshfar, P. Vadrevu, K. H. Lee, and R. Perdisci, "When push comes to ads: Measuring the rise of (malicious) push advertising," ser. IMC '20, 2020, p. 724–737.
- [11] J. Hong, "The state of phishing attacks," *Commun. ACM*, vol. 55, no. 1, p. 74–81, Jan. 2012. [Online]. Available: <https://doi.org/10.1145/2063176.2063197>
- [12] "Google safe browsing," <https://safebrowsing.google.com/>.
- [13] Z. Yang, J. Allen, M. Landen, R. Perdisci, and W. Lee, "TRIDENT: Towards detecting and mitigating web-based social engineering attacks," in *USENIX Security Symposium*. USENIX, 2023.
- [14] S. Abdelnabi, K. Krombholz, and M. Fritz, "Visualphishnet: Zero-day phishing website detection by visual similarity," in *Proceedings of the 2020 ACM SIGSAC Conference on Computer and Communications Security*, ser. CCS '20, 2020, p. 1681–1698.
- [15] Y. Lin, R. Liu, D. M. Divakaran, J. Y. Ng, Q. Z. Chan, Y. Lu, Y. Si, F. Zhang, and J. S. Dong, "Phishpedia: A hybrid deep learning based approach to visually identify phishing webpages," in *USENIX Security Symposium*, 2021, pp. 3793–3810.
- [16] R. Liu, Y. Lin, X. Yang, S. H. Ng, D. M. Divakaran, and J. S. Dong, "Inferring phishing intention via webpage appearance and dynamics: A deep vision based approach," in *31st USENIX Security Symposium (USENIX Security 22)*, 2022, pp. 1633–1650.
- [17] "TensorFlowJS," <https://www.tensorflow.org/js>.
- [18] "Chromium blog: Faster and more efficient phishing detection in m92," <https://blog.chromium.org/2021/07/m92-faster-and-more-efficient-phishing-detection.html>, 2023.
- [19] "Phishtank: Phishing intelligence," <https://phishtank.com/>.
- [20] "Openphish: Phishing intelligence," <https://openphish.com/>.
- [21] "Puppeteer — Puppeteer — pptr.dev," <https://pptr.dev>, [Accessed 13-Jun-2023].
- [22] "puppeteer-extra-plugin-stealth — npmjs.com," <https://www.npmjs.com/package/puppeteer-extra-plugin-stealth>, [Accessed 13-Jun-2023].
- [23] StatCounter, "Desktop Screen Resolution Stats Worldwide, December 2020," <https://gs.statcounter.com/screen-resolution-stats/desktop/worldwide>, [Accessed 21-Jun-2023].
- [24] K. Krippendorff, "Computing krippendorff's alpha-reliability," 2011.
- [25] K. De Swert, "Calculating inter-coder reliability in media content analysis using krippendorff's alpha," *Center for Politics and Communication*, vol. 15, pp. 1–15, 2012.
- [26] "A research-oriented top sites ranking hardened against manipulation - Tranco — tranco-list.eu," <https://tranco-list.eu>, [Accessed 13-Jun-2023].
- [27] J. Deng, W. Dong, R. Socher, L.-J. Li, K. Li, and L. Fei-Fei, "Imagenet: A large-scale hierarchical image database," in *2009 IEEE conference on computer vision and pattern recognition*. Ieee, 2009, pp. 248–255.
- [28] K. Simonyan and A. Zisserman, "Very deep convolutional networks for large-scale image recognition," 2015.
- [29] C. Szegedy, S. Ioffe, V. Vanhoucke, and A. Alemi, "Inception-v4, inception-resnet and the impact of residual connections on learning," in *Proceedings of the AAAI conference on artificial intelligence*, vol. 31, no. 1, 2017.
- [30] K. He, X. Zhang, S. Ren, and J. Sun, "Deep residual learning for image recognition," in *2016 IEEE Conference on Computer Vision and Pattern Recognition, CVPR 2016, Las Vegas, NV, USA, June 27-30, 2016*. IEEE Computer Society, 2016, pp. 770–778. [Online]. Available: <https://doi.org/10.1109/CVPR.2016.90>
- [31] F. Chollet, "Xception: Deep learning with depthwise separable convolutions," in *Proceedings of the IEEE conference on computer vision and pattern recognition*, 2017, pp. 1251–1258.
- [32] S. Bianco, R. Cadène, L. Celona, and P. Napolitano, "Benchmark analysis of representative deep neural network architectures," *IEEE Access*, vol. 6, pp. 64 270–64 277, 2018. [Online]. Available: <https://doi.org/10.1109/ACCESS.2018.2877890>
- [33] "Distributed training with tensorflow," https://www.tensorflow.org/guide/distributed_training.
- [34] B. McMahan and D. Ramage, "Federated learning: Collaborative machine learning without centralized training data," *Google Research Blog*, vol. 3, 2017.

[35] A. G. Howard, M. Zhu, B. Chen, D. Kalenichenko, W. Wang, T. Weyand, M. Andreetto, and H. Adam, "Mobilenets: Efficient convolutional neural networks for mobile vision applications," *CoRR*, vol. abs/1704.04861, 2017. [Online]. Available: <http://arxiv.org/abs/1704.04861>

[36] "puppeteer-extra-plugin-stealth," <https://www.npmjs.com/package/puppeteer-extra-plugin-stealth>.

[37] "PublicWWW - source code search engine," <https://publicwww.com/>.

[38] R. Geirhos, J. Jacobsen, C. Michaelis, R. S. Zemel, W. Brendel, M. Bethge, and F. A. Wichmann, "Shortcut learning in deep neural networks," *CoRR*, vol. abs/2004.07780, 2020. [Online]. Available: <https://arxiv.org/abs/2004.07780>

[39] K. Team, "Keras documentation: Keras Applications — keras.io," <https://keras.io/api/applications/>, [Accessed 21-Jun-2023].

[40] A. Chakraborty, M. Alam, V. Dey, A. Chattopadhyay, and D. Mukhopadhyay, "Adversarial attacks and defences: A survey," *arXiv preprint arXiv:1810.00069*, 2018.

[41] T. Bai, J. Luo, J. Zhao, B. Wen, and Q. Wang, "Recent advances in adversarial training for adversarial robustness," in *Proceedings of the Thirtieth International Joint Conference on Artificial Intelligence, IJCAI-21*, Z.-H. Zhou, Ed. International Joint Conferences on Artificial Intelligence Organization, 8 2021, pp. 4312–4321, survey Track. [Online]. Available: <https://doi.org/10.24963/ijcai.2021/591>

[42] A. Madry, A. Makelov, L. Schmidt, D. Tsipras, and A. Vladu, "Towards deep learning models resistant to adversarial attacks," *arXiv preprint arXiv:1706.06083*, 2017.

[43] J. Rauber, R. Zimmermann, M. Bethge, and W. Brendel, "Foolbox native: Fast adversarial attacks to benchmark the robustness of machine learning models in pytorch, tensorflow, and jax," *Journal of Open Source Software*, vol. 5, no. 53, p. 2607, 2020. [Online]. Available: <https://doi.org/10.21105/joss.02607>

[44] J. Rauber, W. Brendel, and M. Bethge, "Foolbox: A python toolbox to benchmark the robustness of machine learning models," in *Reliable Machine Learning in the Wild Workshop, 34th International Conference on Machine Learning*, 2017. [Online]. Available: <http://arxiv.org/abs/1707.04131>

[45] "TensorFlow.js — Machine Learning for JavaScript Developers — tensorflow.org," <https://www.tensorflow.org/js/>, [Accessed 21-Jun-2023].

[46] M. Z. Rafique, T. Van Goethem, W. Joosen, C. Huygens, and N. Nikiforakis, "It's free for a reason: Exploring the ecosystem of free live streaming services," in *Proceedings of the 23rd Network and Distributed System Security Symposium (NDSS 2016)*. Internet Society, 2016, pp. 1–15.

[47] X. Qi, T. Xie, J. T. Wang, T. Wu, S. Mahloujifar, and P. Mittal, "Towards a proactive ML approach for detecting backdoor poison samples," in *32nd USENIX Security Symposium (USENIX Security 23)*. Anaheim, CA: USENIX Association, Aug. 2023, pp. 1685–1702. [Online]. Available: <https://www.usenix.org/conference/usenixsecurity23/presentation/qi>

[48] T. D. Nguyen, P. Rieger, H. Chen, H. Yalame, H. Möllering, H. Fereidooni, S. Marchal, M. Miettinen, A. Mirhoseini, S. Zeitouni, F. Koushanfar, A. Sadeghi, and T. Schneider, "Flame: Taming backdoors in federated learning," in *USENIX Security Symposium*, 2022. [Online]. Available: <https://api.semanticscholar.org/CorpusID:263886687>

[49] Z. Zhang, X. Cao, J. Jia, and N. Z. Gong, "FIdetector: Defending federated learning against model poisoning attacks via detecting malicious clients," in *Proceedings of the 28th ACM SIGKDD Conference on Knowledge Discovery and Data Mining*, ser. KDD '22. New York, NY, USA: Association for Computing Machinery, 2022, p. 2545–2555. [Online]. Available: <https://doi.org/10.1145/3534678.3539231>

[50] W. Syafitri, Z. Shukur, U. Asma'Mokhtar, R. Sulaiman, and M. A. Ibrahim, "Social engineering attacks prevention: A systematic literature review," *IEEE Access*, vol. 10, pp. 39 325–39 343, 2022.

A. ADDITIONAL DATA

Tables 11 and 12 present additional details about our data collection. Table 11 lists the ad networks we used to find seed URLs, whereas Table 12 shows a detailed breakdown of our dataset in terms of number of images per screen resolution.

TABLE 11: Distribution of Seed URLs across Low-Tier Ad Networks

Ad Network	Seed URLs
Adroll	21716
Adblade	2161
Adpushup	373
Adsupply	205
Pop Ads	178
Adcash	147
AdMaven	118
Ad4Game	42
AdReactor	24
Adsense	15

TABLE 12: The Number of SE attacks and benign page samples per screen resolution

Resolution	# Benign pages	# SE attacks
360x640	2402	255
360x740	-	1481
414x896	3398	24
750x1334	7979	-
768x1024	5067	51
800x1280	4657	61
1024x768	4595	21
1280x800	4162	36
1200x803	8067	-
1366x677	263	11
1366x720	1102	18
1366x724	268	6
1366x728	14530	357
1366x738	1137	22
1366x741	498	9
1366x768	1809	54
1478x837	757	34
1536x816	1364	65
1536x824	14432	474
1536x826	776	25
1536x834	2063	84
1536x864	778	25
1785x993	-	3267
1858x1053	869	30
1858x1080	813	21
1920x998	1960	41
1920x1032	1721	51
1920x1040	16909	502
1920x1050	2354	73
1920x1052	829	19
1920x1080	3195	325
1920x1097	1126	42